Polymer Journal (2019) 51:423–431
https://doi.org/10.1038/s41428-018-0142-7

ORIGINAL ARTICLE

Phase separation during bulk polymerization of methyl methacrylate

Yasuhito Suzuki[1,2,3] · Dylan S. Cousins[2] · Yuya Shinagawa[3] · Robert T. Bell[4] · Akikazu Matsumoto[3] · Aaron P. Stebner[1]

Received: 8 August 2018 / Revised: 16 September 2018 / Accepted: 28 September 2018 / Published online: 2 November 2018

Abstract

We report on the phase separation of methyl methacrylate (MMA) and poly(methyl methacrylate) (PMMA) during bulk free-radical polymerization. The phase separation is induced when the reaction is initiated at room temperature by the redox reaction of benzoyl peroxide in the presence of an amine. During the reaction, the ratio of MMA and PMMA changes continuously. Separation into MMA-rich and PMMA-rich phases coincides with the onset of the Trommsdorff effect. At room temperature, the interface between the two phases remains, even after drying the remaining monomer. When the sample is annealed above the glass transition temperature T_g, the interface disappears. Due to the frozen dynamics of the polymer chains, subsequent cooling below T_g does not result in further phase separation. This result provides evidence for the existence of rich, thermodynamically stable states, which are typically suppressed due to the frozen dynamics of polymers at temperatures below the T_g, after thermal processing above the T_g.

Introduction

Methacrylate polymers, including poly(methyl methacrylate) (PMMA), have applications in the fields of coatings [1], dental fillings [2, 3], and fiber-reinforced composite materials [4, 5]. Because many of the initiators and most of the formed polymers are soluble in the monomer, bulk free-radical polymerization can be conducted [6]. The use of a redox reaction generates radicals under milder conditions (i.e., at room temperature) relative to other types of initiation processes. Although this type of polymerization reaction provides a polymer manufacturing method that does not require postprocess annealing, the high latent heat of polymerization combined with the autoacceleration nature [7–9] (known as the Trommsdorff effect or gel effect) can limit the size scale of components that can be made without boiling the monomer, even in ambient temperature environments [4].

Methyl methacrylate (MMA) and PMMA are understood to be miscible [10]. Phase separation of PMMA and MMA at or above room temperature has not been previously reported in the open literature, likely because of their very slow and complex polymer dissolution kinetics [11, 12]. To dissolve PMMA in MMA at room temperature, the MMA solvent has to diffuse into PMMA and form a rubbery layer on the surface of the glassy PMMA. Chain disentanglement occurs in the rubbery region, and the disentangled polymer molecules can move into the MMA solvent [11]. These processes become extremely slow as the polymer concentration increases. For example, at room temperature, it takes approximately 1 day to dissolve 20 wt% PMMA (Mw = 99 kg/mol, PDI = 1.2) in MMA and ~1 week to dissolve 30 wt% PMMA in MMA. We found that even after

Electronic supplementary material The online version of this article (https://doi.org/10.1038/s41428-018-0142-7) contains supplementary material, which is available to authorized users.

✉ Yasuhito Suzuki
suzuki@chem.osakafu-u.ac.jp

[1] Mechanical Engineering, Colorado School of Mines, 1500 Illinois St., Golden, CO 80401, USA

[2] Chemical and Biological Engineering, Colorado School of Mines, 1500 Illinois St., Golden, CO 80401, USA

[3] Department of Applied Chemistry, Graduate School of Engineering, Osaka Prefecture University, 1-1 Gakuen-cho, Naka-ku, Sakai, Osaka, Japan

[4] National Renewable Energy Laboratory, 15013 Denver W Pkwy, Golden, CO 80401, USA

1 month of stirring, 50 wt% PMMA will not completely dissolve in MMA. The slow kinetics make it difficult to differentiate equilibrium and nonequilibrium thermodynamics. This same issue also arises with many other polymer systems. While the regimes of melt dynamics and dilute-to-semidilute polymer solution dynamics are well defined, there have been few reports regarding the highly concentrated regime [13]. Recently, Tran-Cong-Miyata et al. investigated the MMA/PMMA/poly(ethyl acrylate) (PEA) system and reported a polymerization-induced phase separation via photoinitiation of MMA [14, 15]. In this system, as the reaction proceeds, PMMA is formed, and polymer (PMMA)-polymer (PEA) phase separation takes place. They noticed that the phase separation event has some correlation with the Trommsdorff effect.

In this paper, we investigated bulk free-radical polymerization of MMA [16] using the redox reaction of benzoyl peroxide (BPO) with *N,N*-dimethyl-*p*-toluidine (DMT) as an initiation reaction at room temperature. We found that a phase separation into monomer-rich and polymer-rich phases occurs at the same time as the onset of the Trommsdorff effect. The postprocessing analysis suggests that this phase separation mechanism depends on the path (i.e., temperature and polymer fraction).

Experimental methods

Sample preparation

MMA, DMT, and BPO (Luperox AFR40) were purchased from Sigma-Aldrich. The MMA inhibitor was removed using prepacked column inhibitor removers (Sigma-Aldrich). PMMA (Mw = 99 kg/mol, PDI = 1.2) was obtained from commercial sources and used as received. The molar ratio for the reaction of MMA, DMT, and BPO was 269:1:1. First, DMT was mixed with MMA using a magnetic stirrer for at least 30 min. Subsequently, a total of 6 g of MMA, DMT, and BPO was mixed in a 20 ml scintillation vial. For characterization, the scintillation vial was broken with a hammer. Small samples from the top and bottom were obtained using a wire cutter. To stop the reaction at a certain reaction time, a scintillation vial was frozen in liquid nitrogen. Subsequently, the vial was broken with a hammer, and a sample was taken. Then, the obtained sample (6 g) was dissolved in THF (200 ml). The solution was further diluted in THF (2 mg/ml) for size exclusion chromatography (SEC) measurements.

Temperature measurement using thermocouples

Temperature as a function of time was measured using thermocouples and a data logger from National Instruments. J-Type thermocouples were connected to a 4-Ch thermocouple input (NI 9211), and data were collected with a USB data logger (NI cDAQ-9171). To avoid evaporation, a hole was drilled in a lid with an aluminum backing, and a thermocouple was inserted through the hole. In addition, the gap between the lid and the thermocouple was sealed using vacuum bag sealant tape.

Nuclear magnetic resonance spectroscopy

JEOL ECS-400 and ECX-400 spectrometers were used to record ^{1}H and ^{13}C nuclear magnetic resonance (NMR) spectra, respectively, in deuterated chloroform at room temperature.

Size exclusion chromatography

The number- and weight-averaged molecular weights (M_n and M_w, respectively) were determined by SEC in tetrahydrofuran (flow rate at 0.8 ml/min) as the eluent at 40 °C using a system consisting of a JASCO PU-2080-Plus (pump), JASCO DG-2080–53 (degasser), Chromato Science CS-300 C (thermostat chamber), Tosoh TSK-gel GMHHR-N (column), and JASCORI-2031-Plus (RI detector). The molecular weights were calibrated using standard polystyrenes (Tosoh Corporation, Ltd., Japan).

Thermal analysis

Differential scanning calorimetry (DSC) (TA instruments Q200) measurements were performed with a temperature ramp rate of 10 °C/min and a peak temperature of 160 °C. A second heating cycle was performed after the samples had relaxed to 30 °C; the second heating cycle followed the same conditions as the initial heating cycle. Temperature and enthalpy calibrations were carried out using indium melt. Thermogravimetric analysis (TGA) was performed using TA instruments Q50 at a heating rate of 10 °C/min in a nitrogen stream.

Results and discussion

Figure 1a–o shows selected pictures during the bulk free-radical polymerization conducted in a scintillation vial. After ~70 min of mixing the MMA and initiators, phase separation started at the top of the vial. Approximately 100 min after the initiation of mixing, phase separation occurred in the middle of the vial (Fig. 1d). As captured in Fig. 1f, the phase separation events occurred at different positions in the vial. These phase-separated regions tended to merge. Driven by the density differences, a phase moves up to the top layer (Fig. 1f–k). After ~119 min, the reaction finished,

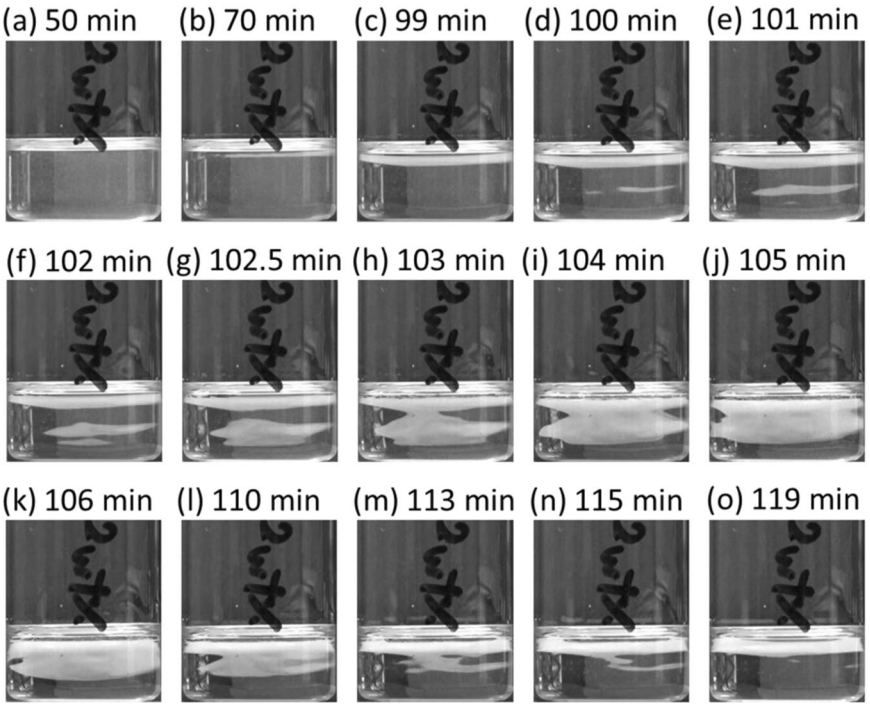

Fig. 1 Selected photographs during the bulk polymerization of PMMA at different times (**a**-**o**) after the initiation of the reaction. The corresponding video is provided in the Supporting Information. The shiny region at the top of the sample is the meniscus

and the interface between the two layers remained. The events captured in Fig. 1e through k occurred within 5 min. Figure 2 shows the temperature profile during the reaction. After initiation, the temperature gradually increased for ~70 min and then increased steeply at the onset of the Trommsdorff effect. Interestingly, phase separation and the Trommsdorff effect coincided. This may suggest that the slowing down of polymer dynamics at a certain concentration causes both the Trommsdorff effect and phase separation. While the phase separation into two layers was the main event, the top layer seemed unstable for a while. Indeed, we often observed further phase separation within the top layer. This instability may be the reason why the top layer appears white in the video and pictures. The second phase separation within the top layer, however, could not be reproduced in the same manner. The reason for this could be the stochastic nature of the event, the sensitive competition between kinetics and thermodynamics, and the complicated redox reaction mechanism of BPO and the amine.

Figure 3 presents the TGA results of the top and bottom layers just after the reaction (120 min after initiation). The 16% weight loss of the top-layer sample at ~100 °C indicates the presence of the remaining MMA. Conversely, there was no clear peak at ~100 °C from the bottom-layer sample. Because ~2% of the weight was lost below 150 °C, a fraction of monomer or oligomer was present in the bottom layer; thus, the top layer was relatively MMA-rich, while the bottom layer was relatively PMMA-rich. Due to the ongoing chemical reaction, the ratio of MMA and PMMA changed continuously, even after the phase

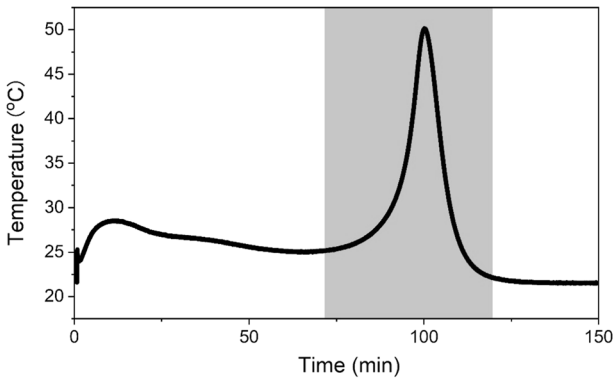

Fig. 2 The temperature profile as a function of time during bulk polymerization. The phase separation was observed in the time range indicated with a purple background

separation. Additionally, evaporation and condensation may have increased the amount of MMA remaining in the top layer. The majority of the remaining polymer burned off between 250 and 420 °C. There were two steps for this burning process (i.e., two maxima from the derivative curve). The low-temperature peak corresponds to the degradation of unsaturated end groups generated by disproportionation, while the higher peak originates from random scissions within the polymer chain [17]. TGA data show that 36.7% and 42.4% of polymer from the top and bottom layers, respectively, contained unsaturated end groups. This slight difference in content may imply a change in the reaction mechanism before and after the onset of the Trommsdorff effect, as discussed later with respect to Fig. 5.

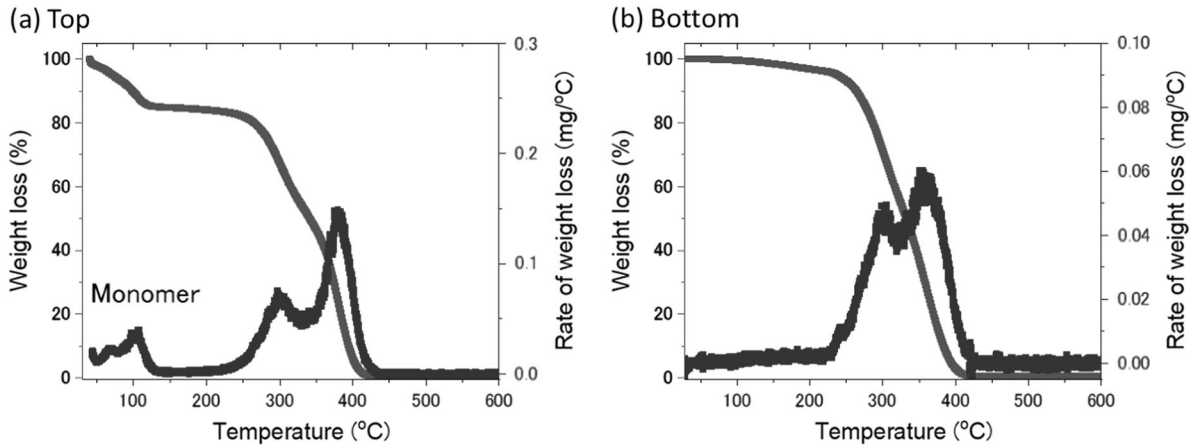

Fig. 3 TGA profile of (**a**) the top and (**b**) bottom layers immediately after the reaction (2 h after initiation). The ~16% weight loss at ~100 °C for the top-layer sample corresponds to the loss of the monomer (MMA). In contrast, almost no monomer was found in the bottom-layer sample

The molecular weight distribution and thermal properties are provided in Fig. 4. Prior to measurements, the top- and bottom-layer samples were kept under vacuum (0.6 kPa) overnight. The molecular weight distributions of PMMA in the top layer and bottom layer measured by SEC are presented in Fig. 4a, c. They are significantly different. Although both layer samples show signatures of bimodal distributions at similar peak positions, the top layer is low-molecular-weight-rich, while the bottom layer is high-molecular-weight-rich. Indeed, the average molecular weights of the top- and bottom-layer samples were 44,000 and 91,400, respectively. In Fig. 4b, d, DSC data are plotted. Because the samples were not annealed, enthalpy relaxation was observed from the first heating as an endothermic peak [18, 19]. It is known that the change in the packing of glass due to physical aging causes enthalpy relaxation [20]. Enthalpy relaxation also depends on the drying process [21]. The value of enthalpy relaxation of the top layer (5.21 J/g) is much higher than that of the bottom layer (0.36 J/g). This indicates that the thermodynamic states of these two glasses are different [22, 23], probably due to the different drying processes resulting in different amounts of the remaining monomer. The glass transition temperatures were obtained from the middle point of the second heating cycle. The top and bottom layers show similar values (Table 1), which is reasonable given that the average molecular weights of both layers were high enough that the effect of the molecular weight on T_g is small [24]. The values are lower than the reported values for PMMA with similar molecular weights because of the effect of the remaining monomers and oligomers [24]. Indeed, the same PMMA sample showed a much higher T_g after purification by reprecipitation (Figure S1). The molecular weight distribution and thermal properties are summarized in Table 1.

To better understand the different molecular weight distributions in the top and bottom layers, the evolution of the molecular weight distribution as a function of reaction time was investigated (Fig. 5). In this experiment, a total of 6 g of the entire sample at different reaction times was frozen in liquid nitrogen and dissolved in the same amount of THF (see Experimental Methods). Separate analyses of the top and bottom layers could not be conducted due to the difficulty of the experiment. Because the monomer did not contribute to the signal, the intensity of the profile increased as the reaction proceeded. Another interesting change was the smooth increase in the average molecular weight up to 60 min after the initiation, which was due to the increase in the viscosity of the sample as the fraction of formed polymer increased. As is the case for uncontrolled radical polymerization in general, the obtained molecular weight was high and the distribution was broad. After 60 min of reaction time, the molecular weight distribution fundamentally changed, corresponding to the onset of the Trommsdorff effect. Due to the frozen dynamics of the polymer, the termination kinetics suddenly slowed down [8, 9]. Thus, the molecular weight of the formed polymer was much higher than that before the onset of the Trommsdorff effect. These data are in good agreement with similar reported measurements [14, 25]. Based on these data, the lower and higher molecular weights of the bimodal molecular distribution correspond to the polymer formed before and after the onset of the Trommsdorff effect, respectively. The negligible indication of a higher molecular weight peak in the top layer (Fig. 4a) implied that the monomer concentration in the top layer was reasonably high and the phase did not reach the onset of the Trommsdorff effect. Once phase separation occurs between lower-molecular-weight PMMA and MMA, the two phases continue to polymerize but are drastically different. Due to the high

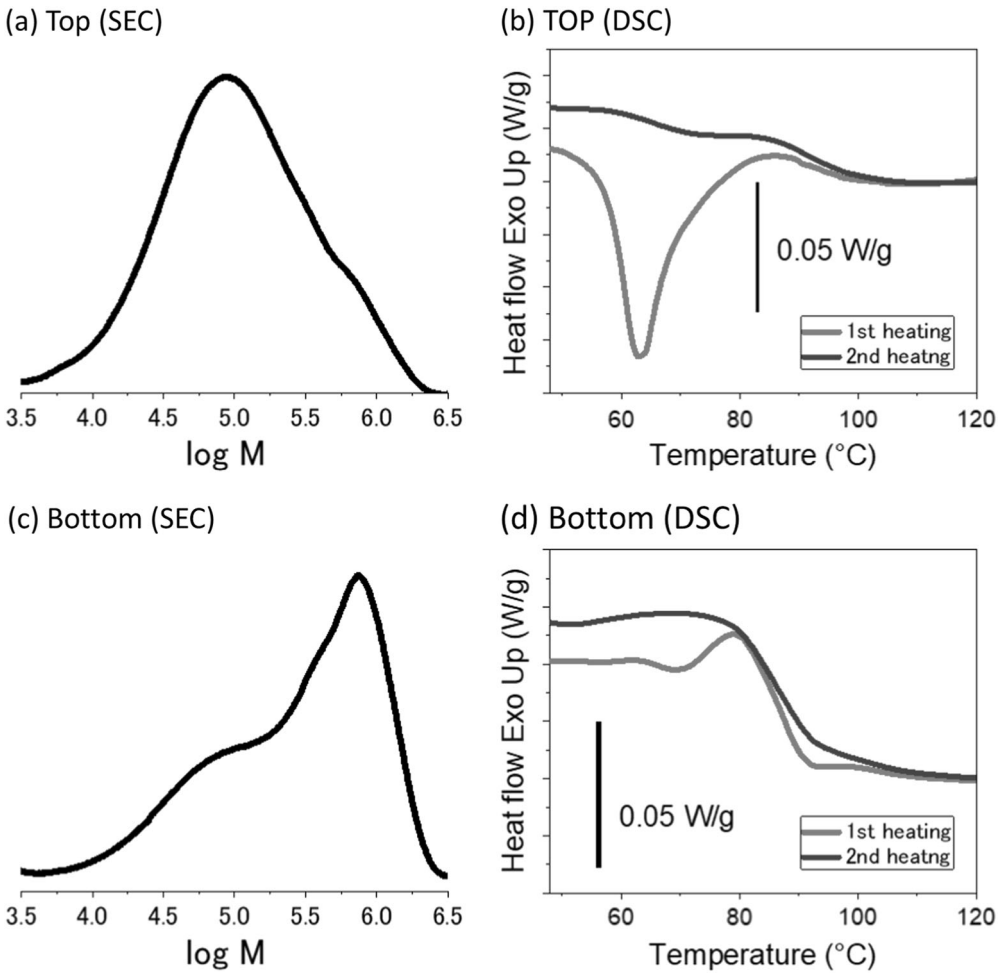

Fig. 4 The molecular weight (M) distribution of the sample from **a** the top layer and **c** the bottom layer obtained from size exclusion chromatography (SEC) with polystyrene standards. Differential calorimetry measurements of **b** the top layer and **d** the bottom layer with a scanning speed of 10 °C/min

Table 1 Summary of molecular weights and thermal properties of the top and the bottom layer sample. $T_{max,\,1}$ and $T_{max,\,2}$ correspond to the low- and high-temperature maxima observed from the derivative data of TGA, respectively. The enthalpy relaxation ΔH_{relax} was obtained from the endothermic peak area around T_g in Fig. 4

	Top layer	Bottom layer
M_n (g/mol)	44,000	91,400
M_w (g/mol)	199,300	455,100
Dispersity	4.53	4.98
$T_{g,\,midpoint}$ (°C)	78.4	79.9
$T_{g,\,midpoint}$ (°C)	128.4 (purified)	127.1 (purified)
$T_{max,\,1}$ (°C)	297.5	298.4
$T_{max,\,2}$ (°C)	379.3	356.2
ΔH_{relax} (J/g)	5.21	0.36

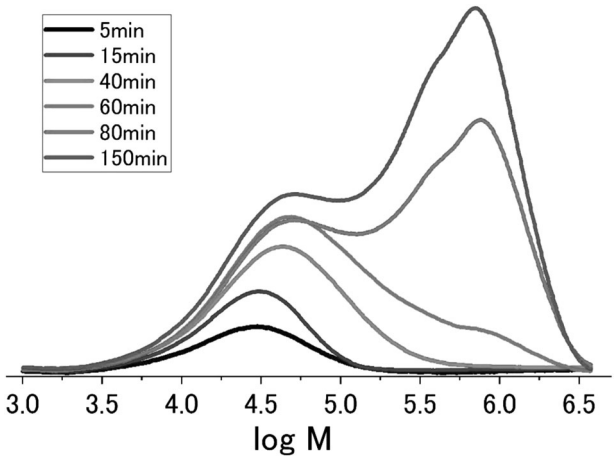

Fig. 5 The molecular weight (M) distributions of the sample at different times from the initiation of the reaction obtained from SEC

concentration of polymer, the bottom layer undergoes the Trommsdorff effect and forms a high-molecular-weight polymer. In the top layer, the relatively lower concentration of polymer dampens the effect of the Trommsdorff effect, and a high-molecular-weight polymer does not form. In the top layer, MMA is consumed both by the reaction and evaporation. In this scenario, the different molecular weight

distributions in the top and bottom layers are a result of the phase separation and are not the driving force of the phase separation.

The formation of PMMA and its tacticity were examined using ^{1}H NMR and ^{13}C NMR. Figure 6 displays the ^{1}H NMR results of (a) the top layer and (b) bottom layer as well as the ^{13}C NMR results of (c) the top layer and (d) bottom layer. Because the reaction is an uncontrolled radical polymerization, the stereochemical structures of the obtained PMMA are atactic. The ratio of the meso (m) and raceme (r) were analyzed using the ^{13}C NMR signal, denoted as "c" in the schematic in Fig. 6a. The indicated three peaks in Fig. 6c, d correspond to the stereochemical structure, (mm), (mr), and (rr), respectively, from the high chemical shift. The integration ratios obtained from the top and bottom layers ((mm)/(mr)/(rr)) were 1.4:33.4:65.2 (top layer) and 1.6:33.2:65.2 (bottom layer). From these ratios, the meso/raceme ratios from the top and bottom layers were found to be 18.1:81.9 (top layer) and 18.2:81.8 (bottom layer). The meso/raceme ratios from the top and bottom layers were similar, suggesting that the stereochemistry is not the cause of the phase separation. The meso/raceme ratio is governed by the reaction environment and temperature [26–28]. The values obtained from our sample are consistent with the literature values, indicating that the temperatures of the top and bottom layers are not significantly different. The meso/raceme ratio was also checked by ^{1}H NMR with ^{1}H, denoted as "b" in the schematic in Fig. 6a. The obtained values are summarized in Table S1. They are in good agreement with the values from ^{13}C NMR.

To further examine the mechanism of the phase separation, we calculated the Gibbs free energy of mixing MMA and PMMA following the classical Flory–Huggins theory based on the lattice model (see Supplemental Information for the procedure). Pairwise interaction energies define the Flory–Huggins interaction parameters (χ). In the lattice model, a polymer is considered as connected repeating units, each of which occupies a single lattice site, similar to a solvent molecule. Phase separation occurs when there is a polymer fraction range where the Gibbs free-energy curve is the upper concave in the plot. Since these χ parameters are somewhat different for the monomer and the polymer, the Flory–Huggins theory predicts phase separation, as shown in Figure S2; however, the temperature predicted (approximately 20 K (−253 °C)) is much lower than that experimentally determined in this study (room temperature, 25 °C). It is common that while the classical Flory–Huggins theory qualitatively predicts phase behavior, the prediction does not agree quantitatively with experiments [13]. The origin of this discrepancy is still debated [29]. H. Tanaka proposed a new type of phase separation, namely, viscoelastic phase separation, that is caused by the presence of slow and fast dynamics in a single system [30, 31]. Given that the dynamics of MMA and PMMA are totally different at room temperature, this phase separation may be caused by the viscoelastic phase separation.

The effect of the treatment after the reaction is discussed with respect to Fig. 7. Immediately after the samples cooled to room temperature, the top layer was still soft (gel-like), while the bottom layer was reasonably hard due to remaining monomer, as detected by TGA (Fig. 3). When the sample was suddenly dried under vacuum or heated above 100 °C (e.g., by placing the vial directly in a 150 °C oven or applying 0.6 kPa for 3 h), voids formed almost exclusively in the top layer because of the sudden boiling of the monomer. Through the Clausius–Clapeyron relation, as pressure decreases, so does the boiling temperature. On the other hand, when the monomer was slowly evaporated at ambient pressure (e.g., by opening the lid and placing the vial in a fume hood for 3 days), the top layer became hard without bubble formation, and the clear interface remained between the top and bottom layers. The interface only disappeared when the sample was annealed overnight at 130 °C, which is above the glass transition temperature [32]. Importantly, once the sample was annealed, phase separation did not occur when the sample was cooled again to room temperature. In other words, the existence of the phase separation mechanism depends on the path (i.e., temperature and polymer fraction) chosen for the sample fabrication.

The concept of these findings is summarized in the schematic shown in Fig. 8. We found polymerization-induced phase separation of PMMA and MMA systems at approximately room temperature. Unlike other polymerization-induced phase separations [14, 15, 33–35], which require more than three chemical species, this phase separation occurs in a monomer/polymer system. Our results imply that the PMMA-in-MMA system has an upper critical solution temperature above room temperature. It is difficult to observe by mixing PMMA in MMA because the dissolution kinetics of PMMA in solution are unreasonably slow for a normal experimental time scale. When the polymer fraction increases as the reaction proceeds, phase separation takes place at a time that coincides with the onset of the Trommsdorff effect. The two phases, however, will never mix at room temperature because of the frozen polymer dynamics. The two phases can mix when annealed above the glass temperature. Once mixed, however, the phases will not separate again upon cooling to room temperature because they are below the glass transition temperature. As depicted in the schematic in Fig. 8, at high polymer fractions near room temperature, the phase formed depends on the path. There are two phases from Path 1, but there is only a single phase from Path 2. Because of the glass transition of the system, the phase of the system

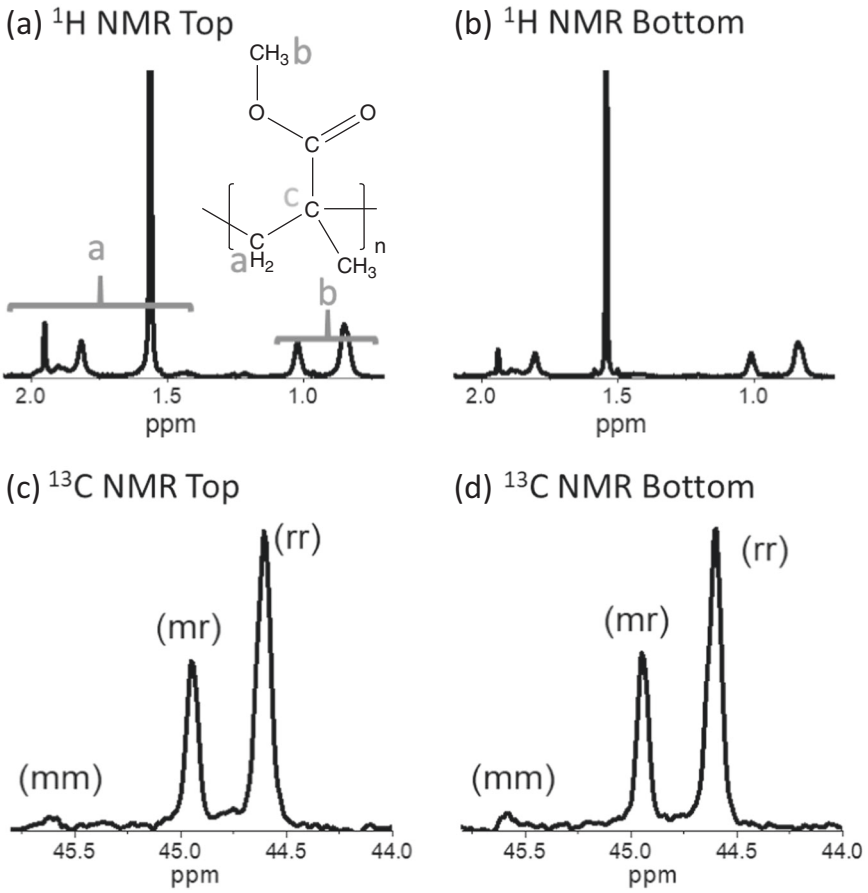

Fig. 6 ^{1}H NMR spectra of the PMMA obtained in **a** the top layer and **b** the bottom layer. Due to the tacticity of the PMMA, protons denoted as "a" and "b" in the schematic generate multiple peaks. The tacticity of the PMMA was analyzed using ^{13}C NMR in **c** the top layer and **d** the bottom layer. These peaks are from ^{13}C and denoted as "c" in the schematic. Three corresponding diads, (mm), (mr), and (rr), where m and r denote meso and raceme, respectively, are indicated

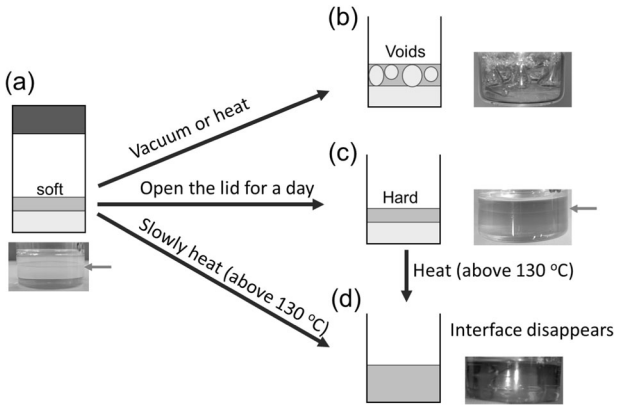

Fig. 7 Schematics and pictures of PMMA samples after the completion of the room temperature reaction (**a**) as well as after different post-processing treatments (**b**, **c**)

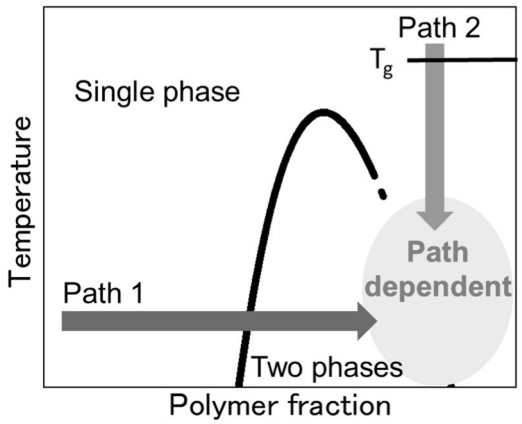

Fig. 8 Schematic of the phase diagram of PMMA in MMA. The highlighted region of the phase diagram represents a part of the phase state that depends upon the processing path: in one case (path 1), there are two phases present, in the other (path 2), the material is a single phase

is governed by kinetics rather than thermodynamics in this region.

Recently, there has been growing interest in complicated phase separation behaviors, especially in biological systems in which there are many proteins in water. Different types of interactions between charges and dipoles complicate the phase stabilities [36]. Other factors, including dynamic heterogeneity [30, 31], temperature gradient, molecular weight distributions, and density differences, may influence the phase separation. Because phase separation affects the fundamental properties of materials (e.g., mechanical, optical, and diffusion kinetics), it is of great importance to better understand the fundamental mechanisms. In this paper, we report a phase separation of a classical and well-

investigated MMA/PMMA system at room temperature. Because the appropriate conditions, including temperature, polymer fraction, and kinetics, need to be satisfied for the phase separation to occur, it has not been documented previously. This finding implies the possibility that rich phase states exist, even in a simple system, that are typically difficult to access due to slow polymer dynamics.

Acknowledgements The authors acknowledge financial support from the State of Colorado Office of Economic Development and International Trade Advanced Industries Program (program manager Katie Woslager) and Colorado Higher Education Competitive Research Authority (CHECRA) through their commitment to the Institute for Advanced Composites Manufacturing Innovation (IACMI) Wind Energy program. This work was supported by the U.S. Department of Energy under Contract No. DE-AC36-08GO28308 with Alliance for Sustainable Energy, LLC, the Manager and Operator of the National Renewable Energy Laboratory. Funding was also provided by the U.S. Department of Energy Office of Energy Efficiency and Renewable Energy Fuel Cell Technologies Office. The authors acknowledge startup funding from Osaka Prefecture University. The authors acknowledge Dr. P.A. Parilla for assistance with DSC. The authors thank Prof. J. Samaniuk, Prof. B. Kappes, and Prof. D. Penumadu for discussions.

Compliance with ethical standards

Conflict of interest The authors declare that they have no conflict of interest.

References

1. Semaltianos NG. Spin-coated PMMA films. Microelectron J. 2007;38:754–61.
2. Ikemura K, Endo T. A review of our development of dental adhesives-effects of radical polymerization initiators and adhesive monomers on adhesion. Dent Mater J. 2010;29:109–21.
3. Achilias DS, Sideridou ID. Kinetics of the benzoyl peroxide/amine initiated free-radical polymerization of dental dimethacrylate monomers: experimental studies and mathematical modeling for TEGDMA and Bis-EMA. Macromolecules. 2004;37:4254–65.
4. Suzuki Y, Cousins D, Wassgren J, Kappes BB, Dorgan J, Stebner AP. Kinetics and temperature evolution during the bulk polymerization of methyl methacrylate for vacuum-assisted resin transfer molding. Compos Part A Appl Sci Manuf. 2018;104:60–67.
5. van Rijswijk K, Bersee HEN. Reactive processing of textile fiber-reinforced thermoplastic composites - an overview. Compos Part A Appl Sci Manuf. 2007;38:666–81.
6. Zoller A, Gigmes D, Guillaneuf Y. Simulation of radical polymerization of methyl methacrylate at room temperature using a tertiary amine/BPO initiating system. Polym Chem. 2015;6:5719–27.
7. Trommsdorff vonE, Köhle H, Lagally P. Zur polymerisation des methacrylsäuremethylesters. Macromol Chem Phys. 1948;1:169–98.
8. Tulig TJ, Tirrell M. Toward a molecular theory of the Trommsdorff effect. Macromolecules. 1981;14:1501–11.
9. Tulig TJ, Tirrell M. On the onset of the Trommsdorff effect. Macromolecules. 1982;15:459–63.
10. Stickler M, Panke D, Wunderlich W. Solution properties of poly (methyl methacrylate) in methyl methacrylate, 1. Viscosities from the dilute to the concentrated solution regime. Macromol Chem Phys. 1987;188:2651–64.
11. Miller-Chou BA, Koenig JL. A review of polymer dissolution. Prog Polym Sci. 2003;28:1223–70.
12. Ouano AC, Carothers JA. Dissolution dynamics of some polymers: solvent-polymer boundaries. Polym Eng Sci. 1980;20:160–6.
13. Rubinstein M, Colby RM. Polymer Physics. Oxford University Press, Oxford; 2006.
14. Ozaki T, Koto T, Nguyen TV, Nakanishi H, Norisuye T, Tran-Cong-Miyata Q. The roles of the Trommsdorff-Norrish effect in phase separation of binary polymer mixtures induced by photopolymerization. Polymer. 2014;55:1809–16.
15. Tran-Cong-Miyata Q, Nakanishi H. Phase separation of polymer mixtures driven by photochemical reactions: current status and perspectives. Polym Int. 2017;66:213–22.
16. Armitage PD, Hill S, Johnson AF, Mykytiuk J, Turner JMC. Bulk polymerization of methyl methacrylate: Part I: some kinetic and modelling considerations for isothermal reactions. Polymer. 1988;29:2221–8.
17. Kashiwagi T, Brown JE, Inaba A, Hatada K, Kitayama T, Masuda E. Effects of weak linkages on the thermal and oxidative degradation of poly(methyl methacrylates). Macromolecules. 1986;19:2160–8.
18. Haque MK, Kawai K, Suzuki T. Glass transition and enthalpy relaxation of amorphous lactose glass. Carbohydr Res. 2006;341:1884–9.
19. Liu Y, Bhandari B, Zhou W. Glass transition and enthalpy relaxation of amorphous food saccharides: a review. J Agric Food Chem. 2006;54:5701–17.
20. Dollimore D. Physical aging in amorphous polymers and other materials. Thermochim Acta. 1982;54:242–3.
21. Descamps N, Palzer S, Zuercher U. The amorphous state of spray-dried maltodextrin: sub-sub-Tgenthalpy relaxation and impact of temperature and water annealing. Carbohydr Res. 2009;344:85–90.
22. Dalal SS, Walters DM, Lyubimov I, de Pablo JJ, Ediger MD. Tunable molecular orientation and elevated thermal stability of vapor-deposited organic semiconductors. Proc Natl Acad Sci USA. 2015;112:4227–32.
23. Dalal SS, Ediger MD. Influence of substrate temperature on the transformation front velocities that determine thermal stability of vapor-deposited glasses. J Phys Chem B. 2015;119:3875–82.
24. Beevers R, White E. Physical properties of vinyl polymers. Trans Faraday Soc. 1960;56:744–52.
25. O'Shaughnessy B, Yu J. Autoacceleration in free radical polymerization. 2. Molecular weight distributions. Macromolecules. 1994;27:5079–85.
26. Matsumoto A. Control of stereochemistry of polymers in radical polymerization. In: Matyjaszewski K, Davis TP, editors. Handbook of Radical Polymerization. New York: Wiley; 2002, Chapter 13, pp 691–773
27. Hatada K, Kitayama T, Ute K. Stereoregular polymerization of α-substituted acrylates. Prog Polym Sci. 1988;13:189–276.
28. Kwei T. The effect of hydrogen bonding on the glass transition temperatures of polymer mixtures. J Polym Sci Part C Polym Lett. 1984;22:307–13.
29. Knychała P, Timachova K, Banaszak M, Balsara NP. 50th anniversary perspective: phase behavior of polymer solutions and blends. Macromolecules. 2017;50:3051–65.
30. Tanaka H. Viscoelastic phase separation. J Phys Condens Matter. 2000;12:R207.
31. Tanaka H. Unusual phase separation in a polymer solution caused by asymmetric molecular dynamics. Phys Rev Lett. 1993;71:3158–61.
32. Hayashi T, Segawa K, Sadakane K, Fukao K, Yamada NL. Interfacial interaction and glassy dynamics in stacked thin

films of poly(methyl methacrylate). J Chem Phys. 2017;146: 203305.
33. Schulze MW, McIntosh LD, Hillmyer MA, Lodge TP. High-modulus, high-conductivity nanostructured polymer electrolyte membranes via polymerization-induced phase separation. Nano Lett. 2014;14:122–6.
34. Girard-Reydet E, Sautereau H, Pascault JP, Keates P, Navard P, Thollet G, Vigier G. Reaction-induced phase separation mechanisms in modified thermosets. Polymer. 1998;39:2269–79.
35. Minakuchi H, Nakanishi K, Soga N, Ishizuka N, Tanaka N. Octadecylsilylated porous silica rods as separation media for reversed-phase liquid chromatography. Anal Chem. 1996;68: 3498–501.
36. Wei MT, Elbaum-Garfinkle S, Holehouse AS, Chen CCH, Feric M, Arnold CB. et al. Phase behaviour of disordered proteins underlying low density and high permeability of liquid organelles. Nat Chem. 2017;9:1118–25.